Metabolic Engineering 69 (2022) 122–133

Contents lists available at ScienceDirect

Metabolic Engineering

journal homepage: www.elsevier.com/locate/meteng

Systematic identification of *Ocimum sanctum* sesquiterpenoid synthases and (−)-eremophilene overproduction in engineered yeast

Xiaomin Deng [a,b,c,1], Bin Shi [b,d,1], Ziling Ye [b], Man Huang [e], Rong Chen [b], Yousheng Cai [b], Zhaolin Kuang [b], Xiang Sun [b], Guangkai Bian [b], Zixin Deng [b,c], Tiangang Liu [b,c,*]

[a] *Ministry of Agriculture Key Laboratory of Biology and Genetic Resources of Rubber Tree/State Key Laboratory Breeding Base of Cultivation and Physiology for Tropical Crops, Rubber Research Institute, Chinese Academy of Tropical Agricultural Sciences, Haikou, 571101, Hainan, People's Republic of China*

[b] *Key Laboratory of Combinatorial Biosynthesis and Drug Discovery, Ministry of Education, Wuhan University School of Pharmaceutical Sciences, Wuhan, 430071, Hubei, People's Republic of China*

[c] *Wuhan Institute of Biotechnology, Wuhan, 470074, Hubei, People's Republic of China*

[d] *Wuhan Drug Solubilization and Delivery Technology Research Center, Wuhan Vocational College of Software and Engineering, Wuhan, 430205, Hubei, People's Republic of China*

[e] *J1 Biotech Co., Ltd., Wuhan 430075, Hubei, People's Republic of China*

ARTICLE INFO

Keywords:
Saccharomyces cerevisiae
Metabolic engineering
Plant sesquiterpene
(−)-Eremophilene
β-caryophyllene
Ocimum sanctum

ABSTRACT

Plant-derived natural active products have attracted increasing attention for use in flavors and perfumes. These compounds also have applications in insect pest control because of their environment-friendly properties. Holy basil (*Ocimum sanctum*), a famous herb used in Ayurveda in India, is a natural source of medical healing agents and insecticidal repellents. Despite the available genomic sequences and genome-wide bioinformatic analysis of terpene synthase genes, the functionality of the sesquiterpene genes involved in the unique fragrance and insecticidal activities of Holy basil are largely unknown. In this study, we systematically screened the sesquiterpenoid biosynthesis genes in this plant using a precursor-providing yeast system. The enzymes that synthesize *β*-caryophyllene and its close isomer *α*-humulene were successfully identified. The enzymatic product of OsaTPS07 was characterized by *in vivo* mining, *in vitro* reaction, and NMR detection. This product was revealed as (−)-eremophilene. We created a mutant yeast strain that can achieve a high-yield titer by adjusting the gene copy number and FPP precursor enhancement. An optimized two-stage fed-batch fermentation method achieved high biosynthetic capacity, with a titer of 34.6 g/L cyclic sesquiterpene bioproduction in a 15-L bioreactor. Further insect-repelling assays demonstrated that (−)-eremophilene repelled the insect pest, fall leafworm, suggesting the potential of (−)-eremophilene as an alternative to synthetic chemicals for agricultural pest control. This study highlights the potential of our microbial platform for the bulk mining of plant-derived ingredients and provides an impressive cornerstone for their industrial utilization.

1. Introduction

Sesquiterpenes and sesquiterpenoids are C_{15} hydrocarbons produced by catalyzing the precursor C_{15} FPP through diverse sesquiterpene synthases and/or enzymes that modify the hydrocarbon chain. Plant-derived sesquiterpenoids have a distinct flavor, fragrance, antimicrobial, attractive, and repellent activities that provide plants survival traits (Chen et al., 2002; Ahmed et al., 2020; Mateos Fernández et al., 2021).

Holy basil (*Ocimum sanctum*) belongs to the Lamiaceae family and is a sacred, traditional medicinal herb that has been used for over more than 3000 years (Gupta et al., 2002). This plant was honored as "The Queen of Herbs", "The Mother Medicine of Nature", and is clearly recorded in Ayurveda and Unani (Rastogi et al., 2015). It was originally distributed in tropical areas, including India, Southeast Asian countries, and the Hainan Province in south China. The medical and healing properties of the plant are complemented by alternative applications, such as in food as a flavorant and aromatic, which increase its commercial value. Modern applications, which include religious, medicinal, culinary, nutritional, aromatic, and ornamental applications, are

* Corresponding author. Key Laboratory of Combinatorial Biosynthesis and Drug Discovery, Ministry of Education, Wuhan University School of Pharmaceutical Sciences, Wuhan, 430071, Hubei, People's Republic of China.
E-mail address: liutg@whu.edu.cn (T. Liu).

[1] These authors contributed equally to this work.

https://doi.org/10.1016/j.ymben.2021.11.005
Received 17 September 2021; Received in revised form 20 October 2021; Accepted 6 November 2021
Available online 12 November 2021

Abbreviations

COSY	homonuclear chemical shift
CSM	complete synthetic medium
DMAPP	dimethylallyl diphosphate
FPP	farnesyl diphosphate
DO	dissolved oxygen
HMBC	heteronuclear multiple bond correlation
HSQC	heteronuclear single-quantum correlation
HR-EI-MS	high resolution electron bombard ionization mass spectrometry
Hyg	hygromycin
IPP	isopentenyl diphosphate
MVA	mevalonate
NMR	nuclear magnetic resonance
NOESY	nuclear overhauser effect spectroscopy
SD	standard deviation
TPS	terpene synthase
VVM	air volume/culture volume/min
YPD	yeast extract-peptone-dextrose
YPDG	yeast extract-peptone-dextrose with galactose

extended by the rich essential oils (Tangpao et al., 2018). Moreover, essential oils from Holy basil have insecticidal, mosquito repellent, and antileishmanial properties and are widely used as food additives and perfumes (Fig. 1). Analyzing the chemical composition of Holy basil essential oil revealed multiple volatile terpenoids, of which sesquiterpenoids are the dominant constituents (Tangpao et al., 2018). Bioactivity assays revealed that some sesquiterpenoids have significant efficacy in controlling agricultural pests and pathogens (Zheljazkov et al., 2008; da Silva et al., 2015).

Genomic sequencing of Holy basil and genome-wide detection of terpene synthase genes have been recently performed (Rastogi et al., 2015; Kumar et al., 2018). However, the products of these genes remain unclear. *Saccharomyces cerevisiae* is generally recognized as a safe (GRAS), robust, and an ideal compatible eukaryotic platform host for the industrial production of high-value terpenoids (Bian et al., 2017; Ma et al., 2019; Shi et al., 2019; Belcher et al., 2020; Ko et al., 2020; Li et al., 2021; Liu et al., 2021). Therefore, we analyzed the function of the Holy basil sesquiterpene synthases. Then, we identified novel or valuable enzymes with fundamental sesquiterpene synthetic elements using the yeast strains YZL141 and JCR27. These two strains provide sufficient amounts of precursors and have been successfully utilized for gene discovery in lycopene biosynthesis, *PTTS* mining (Ma et al., 2019; Chen et al., 2021), and sesquiterpene Guaia-6,10 (14)-diene biosynthesis. This molecule is a building block for the subsequent semisynthesis of plant-derived Englerin A for industrial fermentation (Siemon et al., 2020). These applications encouraged us to use *S. cerevisiae* to systematically screen plant terpenoid synthases.

In this study, we systematically evaluated 14 sesquiterpene synthases from Holy basil and found six active synthases that produce different compounds. The enzymes that synthesize the principal components β-caryophyllene and its isomer α-humulene were successfully identified.

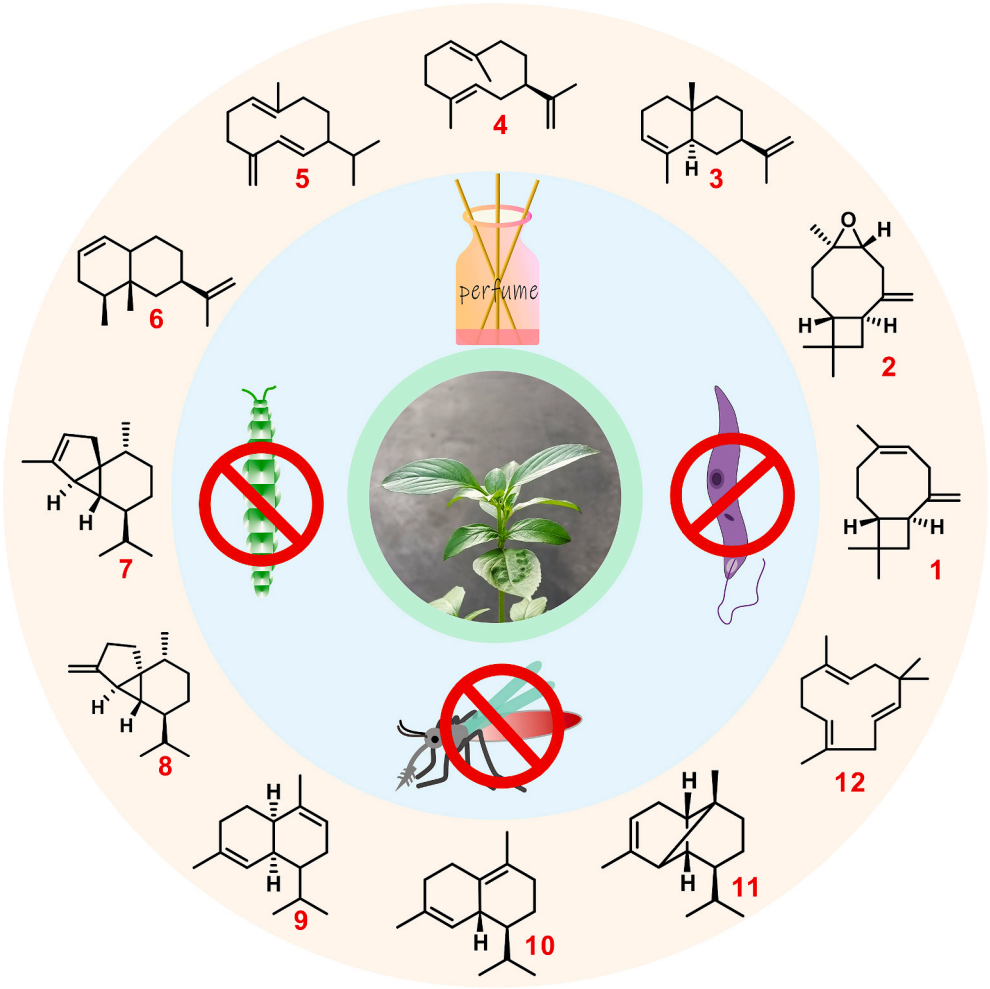

Fig. 1. The major chemical constituents of sesquiterpenoids and bioactivity of the traditional herb Holy basil (*Ocimum sanctum*). Holy basil essential oils have insecticidal, mosquito repellent, and antileishmanial (in purple) properties and are widely used as food additives and perfume. The known major sesquiterpenoids in the derived essential oils (detected by GC-MS) are: 1, β-caryophyllene; 2, caryophyllene oxide; 3, α-selinene; 4, germacrene A; 5, germacrene D; 6, eremophilene; 7, α-cubebene; 8, β-cubebene; 9, α-muurolene; 10, δ-cadinene; 11, α-copaene; and 12, α-humulene. (For interpretation of the references to color in this figure legend, the reader is referred to the Web version of this article.)

Notably, (−)-eremophilene is produced by OsaTPS07 and is a conformer of valencene, which possesses a special scent distinct from valencene. We overproduced this molecule in engineered yeast strains and achieved a milestone titer of 25.5 g/L in a 1-L bioreactor and 34.6 g/L in a 15-L steel fermentor. (−)-eremophilene has repelling activity against the agricultural pest fall leafworm, which suggests that this unusual eremophilene can be a novel alternative valuable chemical for the development of perfume or insect repellant. Our work highlights the great potential of the metabolically engineered microbial platform for bulk mining plant-derived high-value ingredients and lays an impressive cornerstone for industrial utilization.

2. Results

2.1. Bioinformatic analysis of O. sanctum-derived sesquiterpene synthases

The sequenced draft genome of *O. sanctum* and genome-wide detection of terpene synthase genes in Holy basil shed light on the characterization of the roles of terpenes and its clinical therapeutic effects (Rastogi et al., 2015; Jamshidi and Cohen, 2017; Kumar et al., 2018). Since the major terpene components were sesquiterpenes, such as β-caryophyllene, α-cubebene, β-elemene (the thermal conversion product of germacrene A), and α-humulene, we focused on further characterizing the associated sesquiterpene synthases. We carefully analyzed the amino acid (aa) sequences of sesquiterpene synthases using conserved terpene synthase domains (DDXXD/E and NSE/DTE) and amino acid sequence length (510 aa - 600 aa). From this analysis, we selected 11 candidates for comprehensive analysis. These Holy basil sesquiterpene synthases were clustered into three subclades, TPS-a2, TPS-b, and TPS-g (Fig. 2). Apart from OsaTPS44, which lacks the RR $(X)_8W$ motif, the other candidate enzymes possessed conserved motifs (DDXXD/E and NSE/DTE) and one additional RXR motif (Fig. S1).

2.2. Screening Holy basil sesquiterpene synthases using an effective precursor-producing yeast chassis

To functionally characterize the predicted sesquiterpene synthases, the precursor-producing yeast strain YZL141 was transfected with self-

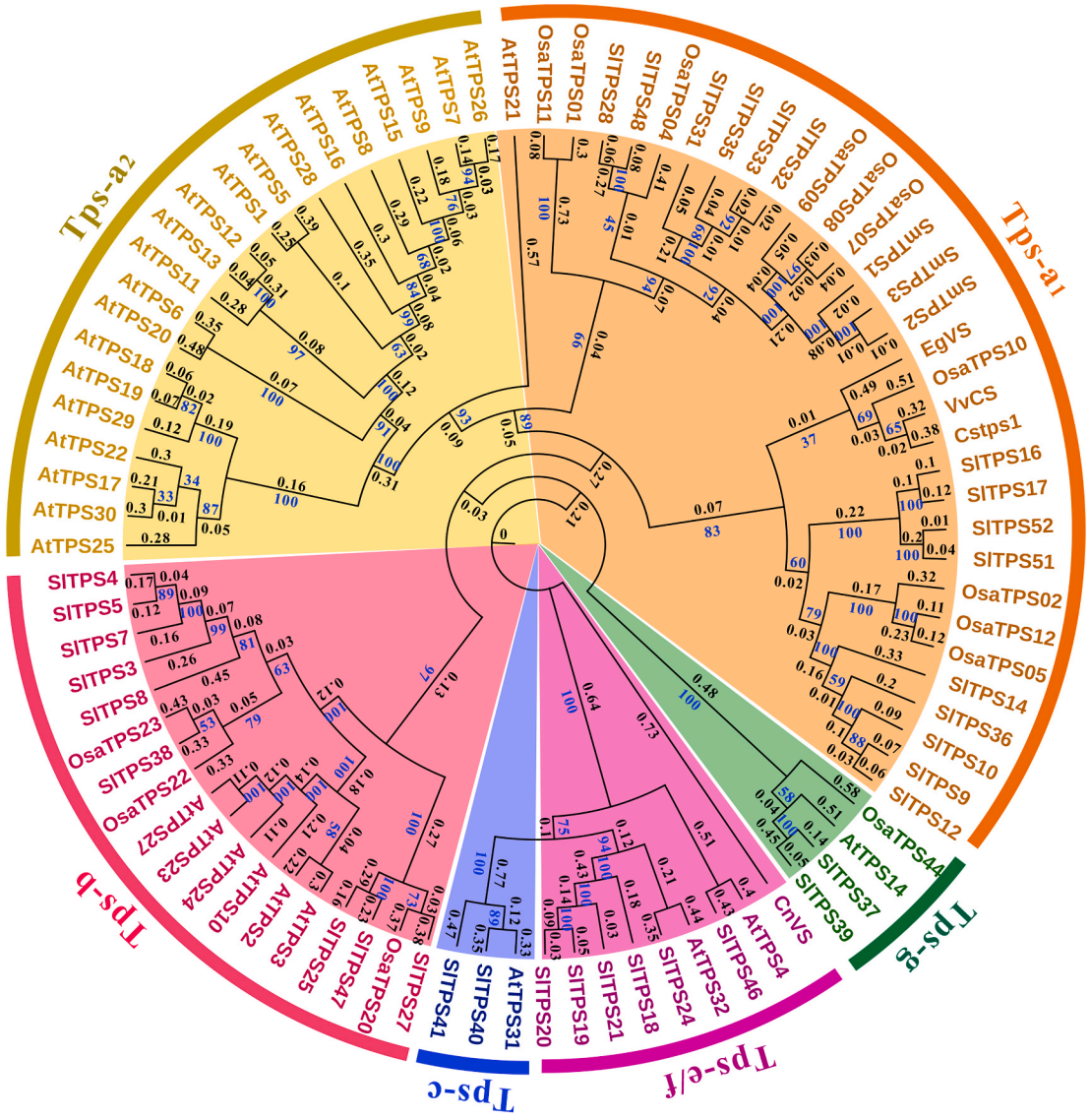

Fig. 2. Phylogenetic analysis of Holy basil, Tomato, and Arabidopsis sesquiterpene synthases. The TPS-a (TPS-a1 and TPS-a2), TPS-b, TPS-c, TPS-e/f, and TPS-g clades are shown in yellow (TPS-a1 represents a distinct clade of Arabidopsis TPS genes) and brown (TPS-a2), pink, blue, purple, and green, respectively. The branch lengths and bootstrap values are presented at the nodes in black and blue, respectively. (For interpretation of the references to color in this figure legend, the reader is referred to the Web version of this article.)

replicating expression vectors containing the synthesized genes (Ma et al., 2019; Chen et al., 2021). Of these, only six enzymes produced sufficient product for gas chromatography-mass spectrometry (GC-MS) analysis (Fig. 3, Figs. S2–S5). Only OsaTPS10 produced multiple sesquiterpenoids. Cadinol, cubedol, and cubenol were the major oxygenated sesquiterpene products. OsaTPS05, OsaTPS02, and OsaTPS12 produced major and minor products. Fortunately, the two major enzymes that synthesize sesquiterpenes in Holy basil, *β*-caryophyllene and *α*-humulene, were identified as OsaTPS02 and OsaTPS12 when compared to standard compound (Fig. S3). In addition, both OsaTPS44 and OsaTPS07 synthesized the main product. The product generated by OsaTPS44 was *trans*-nerolidol was identified via retention time and mass peaks, which were in line with the standards. However, the product generated by OsaTPS07 (hereafter designated as compound I) was difficult to determine because its retention time (14.34 min) did not match valencene (14.40 min), despite the mass peaks being highly similar (Fig. S6). Compound I might be a novel sesquiterpene with a chemical structure that is highly similar to that of valencene, and requires further investigation. Most impressively, the smell from the engineered yeast strain harboring the *OsaTPS07* gene was distinct from the scents emitted from the other engineered strains, which prompted us to identify its exact chemical properties and biological features.

2.3. In vitro enzymatic reaction of OsaTPS07 with precursor FPP

In vitro enzymatic reactions were analyzed by mixing the purified recombinant OsaTPS07 protein with the direct substrate FPP to verify OsaTPS07 function *in vivo*. A clear peak that was identical to the one in the *in vivo* experiment emerged in the GC-MS result of the OsaTPS07-supplemented sample (Fig. 4, Fig. S6). In the *in vivo* and *in vitro* assays, similar retention times and highly similar mass fragments of the OsaTPS07 enzymatic product were observed, which prompted us to resolve its chemical structure and evaluate its features.

2.4. Engineering yeast to overproduce the OsaTPS07 enzymatic product

To obtain an adequate amount of compound I for chemical structure analysis, we integrated the *OsaTPS07* gene into the precursor-enhancing JCR27 yeast strain and iteratively engineered the mutant strain to realize the full potential of OsaTPS07 in a heterologous and highly adaptable system (Siemon et al., 2020) (Fig. 5A). First, the biosynthetic *OsaTPS07* gene was combined with the *ERG20* gene using the GAL promoter. This construct was incorporated into the *leu2* locus to generate the JHM1 mutant strain (Fig. 5B and C). Owing to the FPP precursor synthesized via the ERG20 enzymatic polymerization of IPP and DMAPP *in vivo*, coupled with OsaTPS07 catalytic activity, we concentrations up to 231.4 mg/L of compound I in shake-flask conditions (Fig. 5C). Increasing the gene copy number to enhance its expression is an effective strategy for strengthening target metabolic pathway flux (Xie et al., 2015; Ma et al., 2019). An additional *OsaTPS07* gene was added to the *ura3* locus of JHM1 to generate the JHM2 mutant strain. As a result, the compound I titer was significantly increased to 394.8 mg/L in JHM2, approximately 1.7 times higher than the original JHM1 strain using shake-flask conditions. Deleting the *hyg-resistance* gene in JHM2 to generate the JHM3 mutant did not significantly affect the compound I titer. To further boost the titer, an extra copy of the *OsaTPS07* gene combined with the *hyg* gene was inserted into the *gal80* site of the JHM3 chromosome, and the recombinant strains were screened on hygromycin-containing plates. The surviving mutant strain with the correct disruption of the *gal80* gene was designated JHM4, which was induced by glucose deprivation instead of high galactose levels, sharply reduced the manufacturing cost. The compound I titer increased to 576.5 mg/L, indicating that the transcript level of the *OsaTPS07* gene in these mutants was a vital factor for target compound biogenesis. After recovery of the auxotrophic genes *URA* and *TRP*, the final engineered strain JHM5 was constructed. The compound I titer in this strain increased to 708.5 mg/L in shaken flasks (Fig. 5C). Two major factors may have contributed to this high titer. The most important one is the high purity of the OsaTPS07 enzyme and its high specific activity in converting the precursor FPP, which was quite different from the multiple products observed after transformation with valencene synthase and patchoulol synthase (Beekwilder et al., 2014; Liu et al., 2021). Second, the robust yeast platform is highly suitable for OsaTPS07 expression. Thus, we exploited the advantages of the yeast system and the heterologous enzyme *in vivo* (Zhang et al., 2020). Other strategies using the current mutant strain JHM5 may improve present productivity using shake flasks Liu et al., 2021.

2.5. Structural characterization revealed the OsaTPS7 product as (−)-eremophilene

Compound I was a colorless, amorphous oil. Based on the HR-EI-MS data ($[M]^+$ ion at *m/z* 204.18721, calcd. 204.18725) (Fig. 6A), the molecular formula was established as $C_{15}H_{24}$, requiring four degrees of

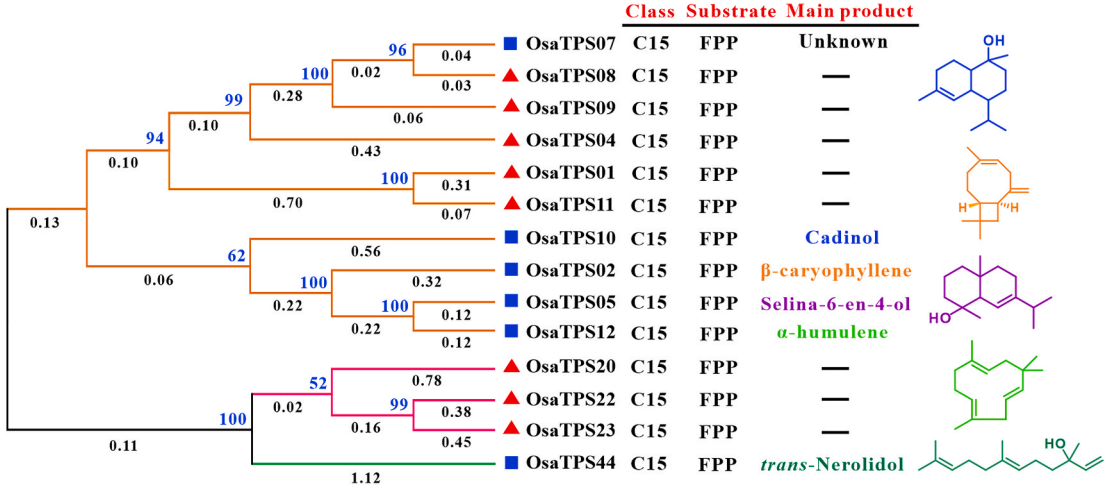

Fig. 3. Phylogenetic analysis and the function of the Holy basil sesquiterpene synthases. The main functional products of the Holy basil sesquiterpene genes are listed and represented in distinct colors: cadinol, OsaTPS10, in blue; *β*-caryophyllene, OsaTPS02, in brown; selina-6-en-4-ol, OsaTPS05, in purple; *α*-humulene, OsaTPS12, in bright green; *trans*-nerolidol, OsaTPS44, in dark green. The branch lengths and bootstrap values are presented at the nodes in black and blue, respectively. (For interpretation of the references to color in this figure legend, the reader is referred to the Web version of this article.)

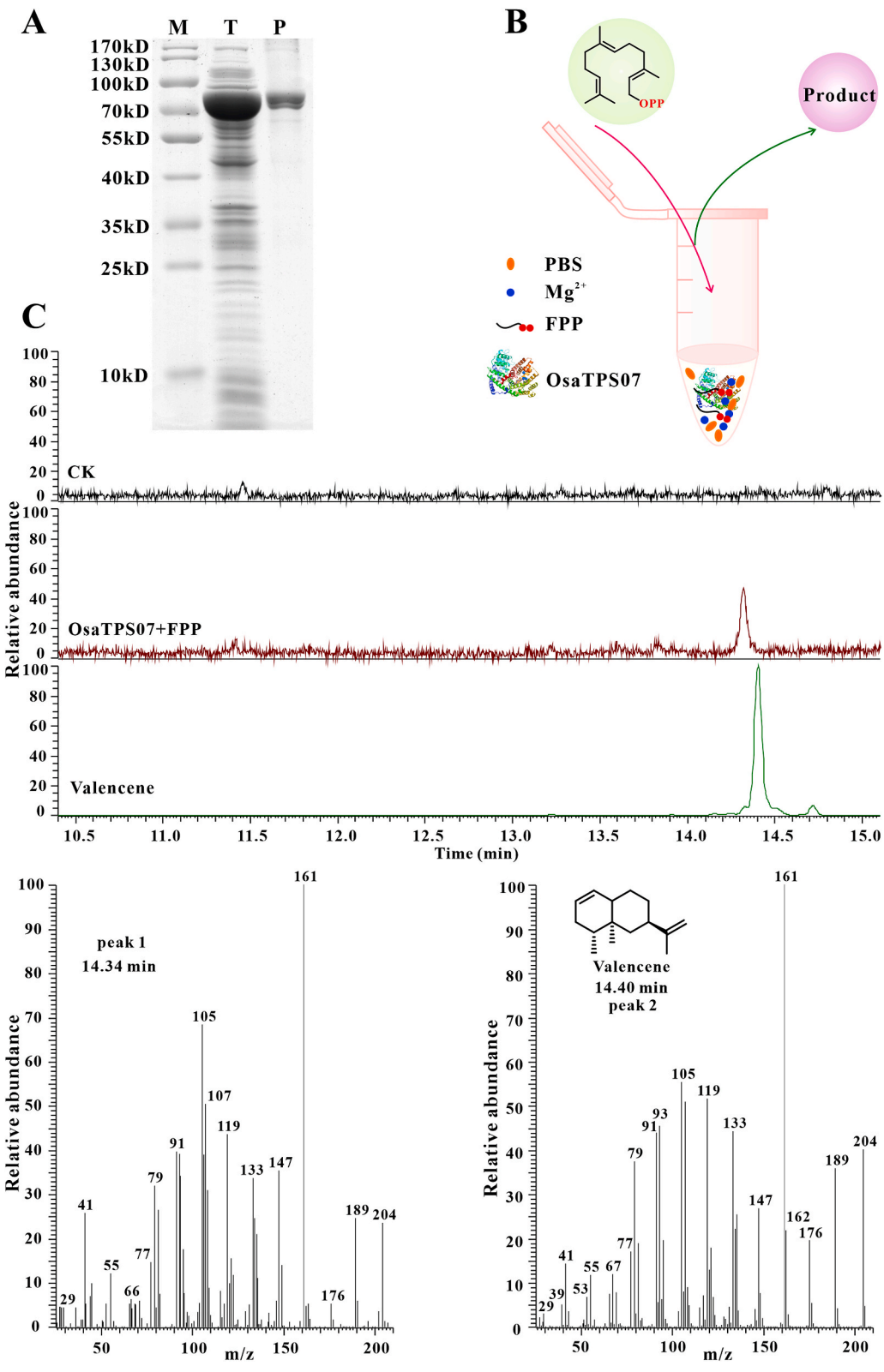

Fig. 4. *In vitro* analysis of OsaTPS07 enzyme function. (A) Purified OsaTPS07 protein from recombinant *Escherichia coli*. M refers to the protein marker, T refers to the total cell disruption components, P refers to the purified recombinant OsaTPS07 protein. (B) *In vitro* reaction system used to detect OsaTPS07 enzymatic function. (C) GC spectrum and the corresponding mass spectra of the OsaTPS07 enzymatic product. Peak 1 represents the product synthesized by OsaTPS07 reacting with the substrate FPP. Peak 2 represents the valencene standard.

unsaturation. Analysis of ^{1}H, ^{13}C NMR, and HSQC data (Table 1) revealed that this metabolite possessed three nonprotonated carbons (including two sp2 carbons), three methines (including an sp2 carbon), seven methylenes (including an sp2 methylene), and three methyl groups. Further analysis of the 2D NMR data (Fig.6B, Figs. S7–S12) revealed that compound I shared the same planar structure as (+)-eremophilene (Schifrin et al., 2015; Burkhardt et al., 2016). A detailed comparison of the 1D and 2D NMR data of compound I with those of (+)-eremophilene revealed that they were identical. However, their specific rotation values were opposite to one another {1: $[\alpha]_D^{20}$-113.4 ($c = 0.28$, $CHCl_3$); (+)-eremophilene: $[\alpha]_D^{25}$ +131.7 ($c = 1.00$, $CHCl_3$)}. Thus, compound I was determined to be the enantiomer of

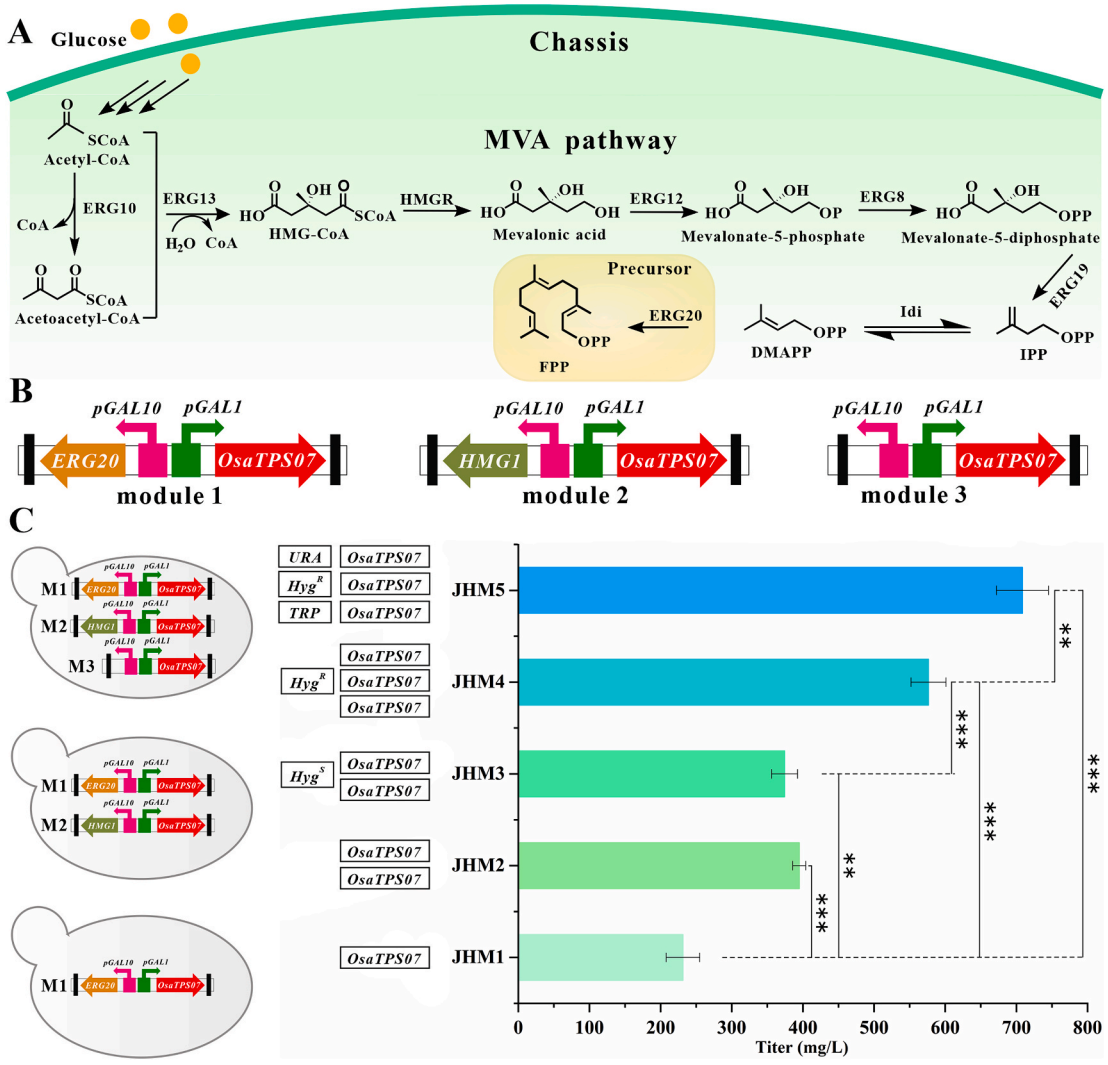

Fig. 5. The titer of compound I in iterative mutant yeast strains in shake flasks. (A) The MVA pathway in the yeast system. The present chassis that produced the FPP as the precursor for the subsequently engineered mutants to overproduce the sesquiterpene of interest (Compound I, the enzymatic product of OsaTPS07); (B) The gene modules constructed for integrated expression. These expression modules were respectively integrated into the chromosomal sites of *leu2* (module 1, Chromosome III), *ura3* (module 2, Chromosome V), and *gal80* (module 3, Chromosome XIII); (C) The copy numbers of *OsaTPS07* and the auxotrophic genes in the iterative mutants. The engineered strain JHM1 that contained the expression module 1 (abbreviate as 'M1') has one copy of the *OsaTPS07* gene. The engineered strains JHM2 and JHM3 that contained the expression module 1 ('M1') and module 2 ('M2') have two copies of the *OsaTPS07* gene. The engineered strains JHM4 and JHM5 that contained the expression module 1 ('M1'), module 2 ('M2') and module 3 ('M3') have three copies of *OsaTPS07*. $^{*}P < 0.05$; $^{**}P < 0.01$; $^{***}P < 0.001$ (Student's t-test: two-tailed, two-sample equal variance).

(+)-eremophilene. Eight conformational isomers involving (−)-eremephilene were predicted, as this eudesmane-type sesquiterpene harbors three chiral centers. The compound produced by OsaTPS07 will enhance our understanding of the enzymatic biosynthesis mechanism of these eight enantiomers.

2.6. High-density fermentation for (−)-eremophilene overproduction

To match the characteristics of the GAL promoters used to control (−)-eremophilene synthesis genes in the construction of strain JHM5 (the GAL promoter is turned off in the presence of glucose and turned on when glucose is absent), the fermentation process was divided into two stages. The main purpose of the first feeding stage was the rapid growth of the strains. The products began to accumulate rapidly in the second feeding stage. Using this two-stage fermentation, a balance between healthy growth and product accumulation was achieved.

Given that the demand for O_2 increases during the growth of the engineered strains in fermenters, oxygen supply was increased by setting the agitation speed to 200–700 rpm and controlling the ventilation from 1 to 2 vvm (air volume/culture volume/min, VVM) for the 1-L parallel bioreactors. Since the 1-L parallel bioreactor that we used was made of glass, which cannot be pressurized like a steel tank, the dissolved oxygen (DO) in the 1-L bioreactor at the late stages of fermentation was generally retained at a lower level from 0 to 10%. The final fermentation cycle of the 1-L parallel bioreactor was thus longer than that of the steel tank, and the titer of (−)-eremophlilene reached 25.5 g/L (Fig. 7A and B). This result demonstrates the excellent high-yield performance of the engineered strain. In the 15-L steel tank, in addition to increasing the agitation speed and adjusting the ventilation volume, we also increased the oxygen supply through the regulation of tank pressure. Tank pressure at the beginning of the reaction was set to 0 MPa and was allowed to reach a maximum value of 0.04 MPa. The DO in the 15-L steel tank in the late stages of fermentation was maintained between 10% and 30%, providing adequate oxygen for the desired fermentation. Thus, enlarging the fermentation scale using a 15-L steel tank (Fig. 7C and D) revealed that the strain performance in this volume is still very good.

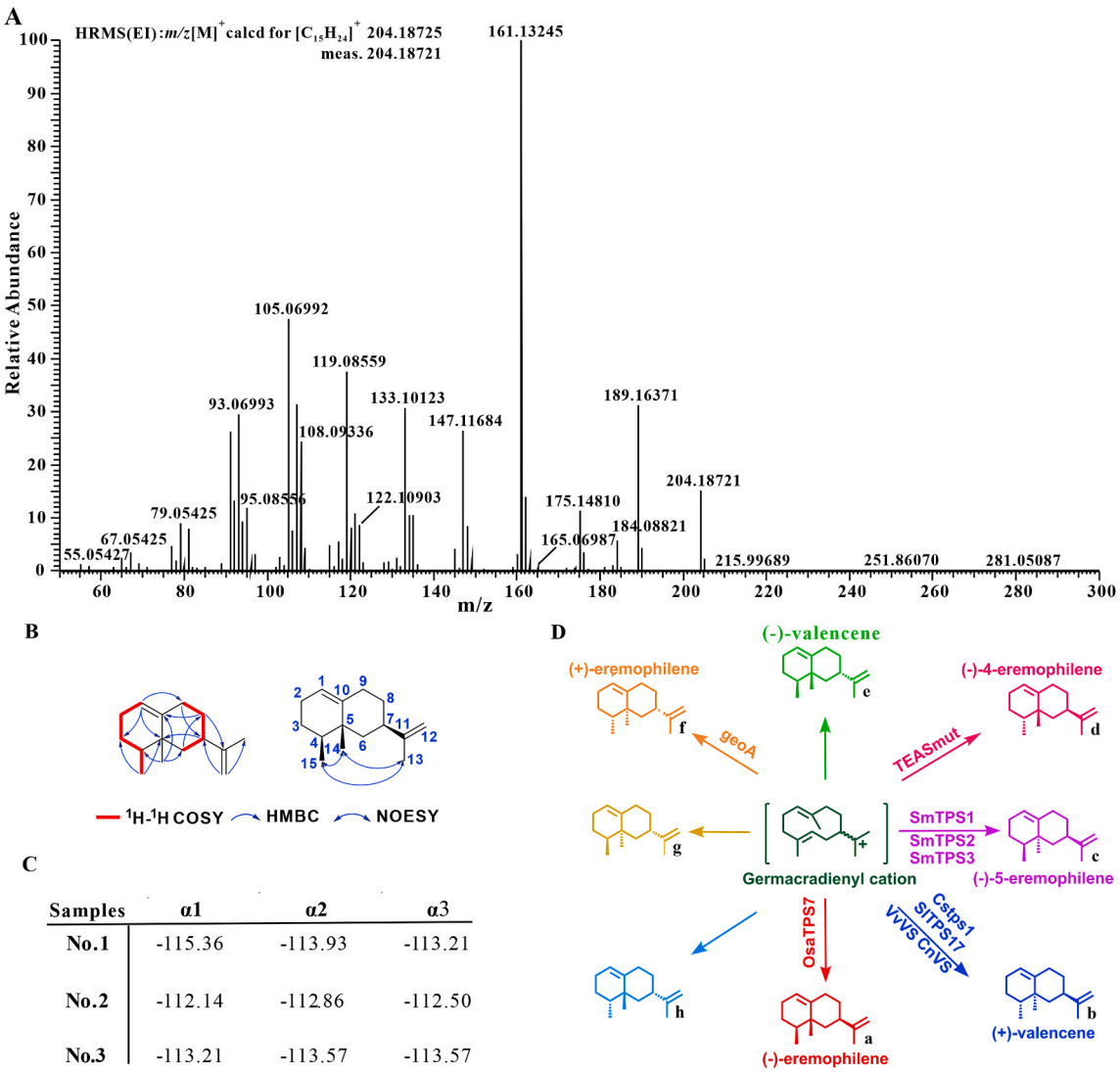

Fig. 6. Structural characterization of the OsaTPS07 product. (A) HR-EI-MS spectrum of compound I; (B) The key ^{1}H–^{1}H COSY, HMBC and NOESY correlations of compound I; (C) The optical specific values of compound I. Triplicate measurements were performed in three independent biological experiments. α1, α2 and α3 represent the optical specific values of the three samples; (D) The eight theoretical epimers of eudesmane-type sesquiterpenes are represented in red (a), blue (b), purple (c, Xie et al., 2015), pink (d), green (e, Coates and Shaw, 1970), orange (f), yellow (g, Zhao et al., 2004a, CAS# 851936-59-9), and cyan (h), respectively, in which OsaTPS07 produced (−)-eremophilene (compound I, a), which is identified in the present study for the first time. (For interpretation of the references to color in this figure legend, the reader is referred to the Web version of this article.)

Table 1
^{1}H NMR (600 MHz, $CDCl_3$) and ^{13}C NMR (150 MHz) data for compound I in $CDCl_3$.

Position	δ_H	δ_C
1	5.36 (dt, J = 4.4, 2.1 Hz)	120.4 d
2	2.03 (m); 1.96 (m)	25.4 t
3	1.45 (m)	27.1 t
4	1.51 (m)	37.0 d
5	–	38.0 s
6	1.54 (d, 7.6)	39.7 t
7	2.05 (m)	38.5 d
8	1.68 (m)	30.1 t
9	2.40 (m); 1.96 (m)	28.4 t
10	–	144.0 s
11	–	149.9 s
12	4.72 (s); 4.75 s	108.2 t
13	1.74 (s)	21.5 q
14	0.93 (s)	20.2 q
15	0.87 (d, 6.5)	16.0 q

Moreover, the pressure of the steel tank maintained the DO level, which accelerated the life cycle of the JHM5 strain. As shown in Fig. 7C, the fermentation cycle was shortened to approximately 90 h, and the titer increased to 34.6 g/L, which is the highest reported yield to date. Our results were comparable to those of industrial production methods and were close to the industrial production level of the sesquiterpene amorphadiene (40 g/L) (Westfall et al., 2012). This study thus developed a new method for the future industrial production of (−)-eremophilene and provided new insights for the studies of other similar high-value products of plant origin.

2.7. Characterization of the fragrance properties and bioactivity of (−)-eremophilene

2.7.1. (−)-Eremophilene emits the unique aroma different to (+)-valencene

To assess the potential value of (−)-eremophilene as a flavoring agent, we analyzed the aromatics from this molecule. The aroma was a mix of leathery, woody, and herb scents. White smoke arose along with an enhanced smell when the compound was heated, suggesting that it

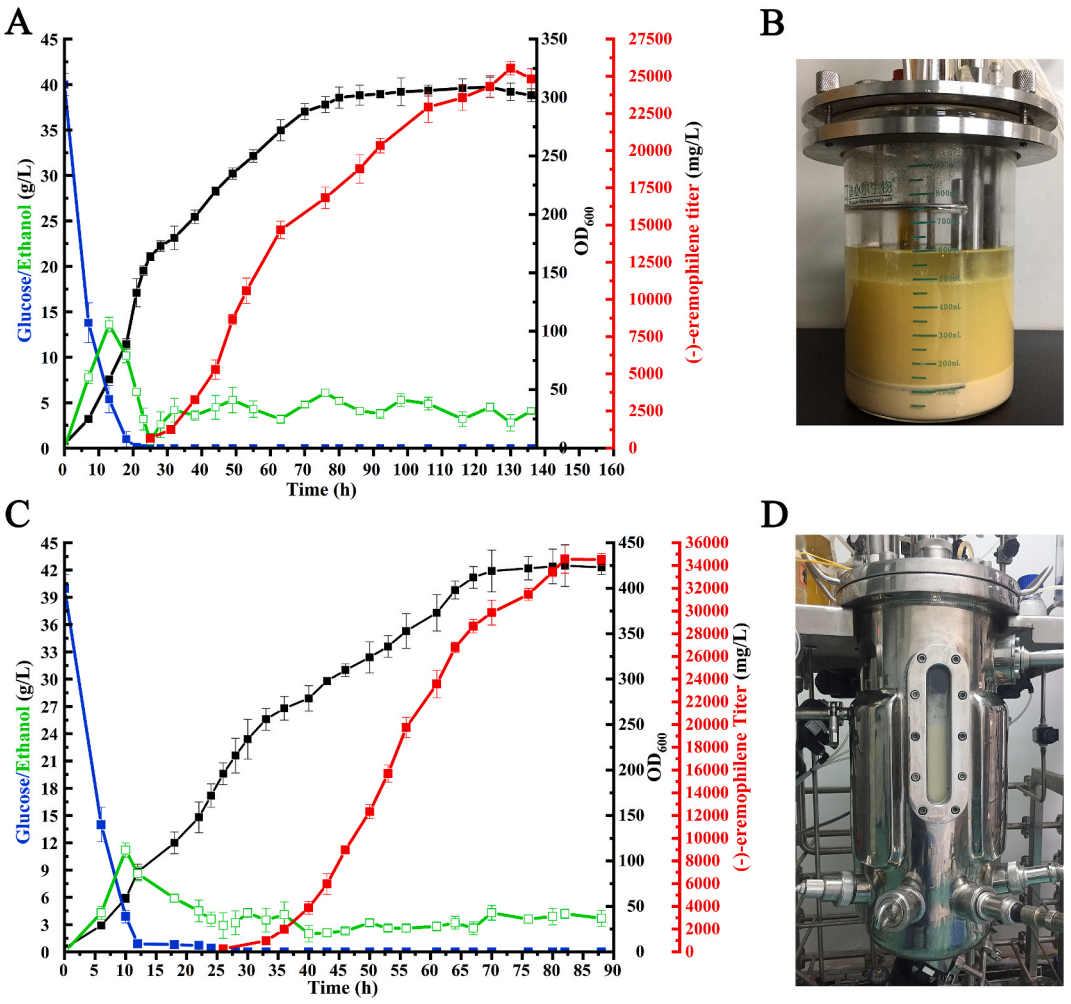

Fig. 7. Optimization of fed-batch fermentation of JHM5. High-density fermentation of strain JHM5 for (−)-eremophilene production. (A) Result of fermentation in a 1-L parallel bioreactor. Time course of cell growth, (−)-eremophilene production, and residual concentrations of glucose and ethanol during fed-batch fermentation were recorded. Error bars indicate the standard deviations of three biological replicates. (B) Fermentation broth in the 1-L bioreactor. The upper oil phase contains estergel and (−)-eremophilene. (C) Result of fermentation in 15-L fermentor. (D) A photo of the 15-L fermentor in operation.

could be used as a base note ingredient and food flavor agent. This unique fragrance was completely different from that of (+)-valencene, which was evaluated and confirmed by a flavorist from the Flavor & Fragrance Company (personal communication). Combined with the moderate content of (−)-eremophilene in Holy basil, this unique fragrance may play a fixative role in the fragrance of *O. sanctum*.

2.7.2. *Volatile (−)-eremophlilene repels third instar Spodoptera frugiperda larvae*

Sesquiterpenoids protect plants against insect infestation (Alquézar et al., 2021; Mateos Fernández et al., 2021). In particular, (−)-5-epieremophilene, an enantiomer of (−)-eremophilene, is a deterrent to the pest, cotton bollworm (*Helicoverpa armigera*) (Luo et al., 2020). Another pest, fall leafworm (*Spodoptera frugiperda*), which belongs to the Noctuidae family, causes significant damage to crop production in China. Our results showed that the feeding areas of leaves after (−)-eremophilene treatment were significantly lower than those of control leaves (Table S4, Fig. S15). The repellant effect of (−)-eremophilene was as high as approximately 90% using 50 μg/mL (−)-eremophilene (Fig. 8). These data suggest that this plant-derived compound possesses an insect repellent activity and could represent an alternative green antifeedant to insect pests. Therefore, (−)-eremophilene, an active ingredient in Holy basil, confers a distinctive fragrance and effective bioactivities.

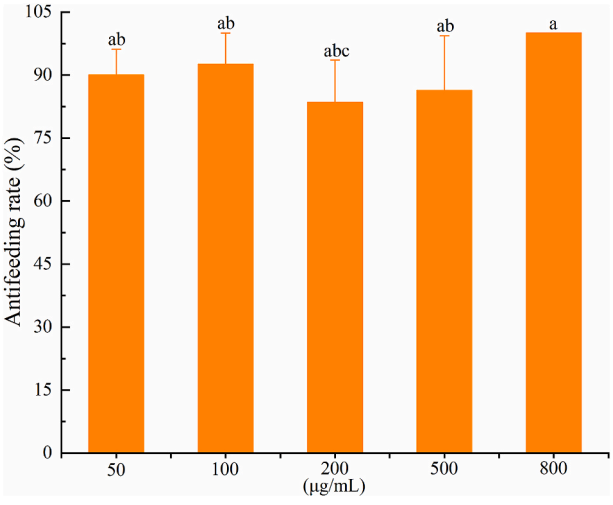

Fig. 8. The antifeedant activity of (−)-eremophlilene against third instar *Spodoptera frugiperda* larvae. Data are mean ± SE. Each treatment was tested with five replicates. Different letters above the columns indicate significant differences (at $P < 0.05$ level). Statistical differences were analyzed using Duncan's new multiple range test.

3. Discussion

In this study, we developed an approach to systematically identify the genes involved in sesquiterpenoid biosynthesis in the traditional herb, Holy basil, by heterologous expression in an efficacious precursor-producing yeast system. Compared with traditional methods utilizing prokaryotic expression and *in vitro* reactions or transgenic over-expression in model plants to identify plant terpene synthases (Falara et al., 2011; Zhou and Pichersky, 2020), our strategy expedites the identification of plant-derived terpene synthases and can realize the potential industrial production of natural compounds.

Using this rapid strategy, we successfully identified the genes involved in the biosynthesis of β-caryophyllene and its close isomer α-humulene, *OsaTPS02* and *OsaTPS12*, respectively. β-caryophyllene and α-humulene are the major terpene constituents that are responsible for the principal aromas emitted from *O. sanctum* leaves (Tangpao et al., 2018). These two compounds also possess potent oviposition deterrent effects against *Aedes aegypti* (da Silva et al., 2015) and effective anti-leishmanial activity (Zheljazkov et al., 2008). The existence of *OsaTPS02*, *OsaTPS12*, and their catalytic products can partly explain the characteristic fragrance of Holy basil and its antileishmanial efficacy. Therefore, *OsaTPS02* and *OsaTPS12* are novel gene resources for generating these two valuable compounds. To the best of our knowledge, *trans*-nerolidol has not been identified in Holy basil extracts (Zheljazkov et al., 2008; Padalia and Verma, 2011; Tangpao et al., 2018). The evidence that OsaTPS44 generates *trans*-nerolidol indicates that *OsaTPS44* expression is strictly controlled in *O. sanctum*. A similar biological phenomenon involving (−)-5-epieremophilene is observed in *Salvia miltiorrhiza* (Fang et al., 2017). Since *trans*-nerolidol has antioxidant, antibacterial, and antifungal activities, the protective roles of the *OsaTPS44* gene in Holy basil need further investigation.

(−)-eremephilene was first reported in *Petasites albus* in 1968 (Krepinsky et al., 1968). However, its characterization and application are largely hindered by its low concentration in plants, and the enzymes that synthesize this specific compound are largely unknown. (−)- eremephilene theoretically has eight conformational isomers, since this eudesmane-type sesquiterpene harbors three chiral centers (Zhao et al., 2004b; Xu and Dickschat, 2020). Of these, four conformational isomers have been identified (Sharon-Asa et al., 2003; Lücker et al., 2004; Greenhagen et al., 2006; Bleeker et al., 2011; Beekwilder et al., 2014; Schifrin et al., 2015; Burkhardt et al., 2016; Fang et al., 2017). The enzymes responsible for the biosynthesis of the other four isomers remain unclear. The Holy basil OsaTPS07 enzyme identified in the present work was found to synthesize (−)-eremophilene for the first time. The discovery of (−)-eremophilene-synthesizing enzymes will help elucidate the biosynthetic mechanisms of additional conformational isomers. OsaTPS7 from Holy basil exhibited extraordinarily high purity and high activity, making it an excellent biosynthetic element. It facilitated the biosynthetic ability of the optimized yeast mutant JHM5. The full potential of JHM5 productivity was realized during fed-batch fermentation. In literature reports (Table S5), the highest titer of linear sesquiterpene β-farnesene reached approximately 130 g/L in *S. cerevisiae* and was achieved by Amyris (Meadows et al., 2016). The highest reported titer of its isomer, α-farnesene, is 10.4 g/L in *S. cerevisiae* (Wang et al., 2021). Recently, another linear sesquiterpene *trans*-nerolidol was produced at a titer of 7.01 g/L (Li et al., 2021). In addition, the highest titer of the bicyclic sesquiterpene amorpha-4, 11-diene, that is 40 g/L, was also reported by Amyris (Westfall et al., 2012; Paddon et al., 2013). Our (−)-eremophilene, the bicyclic sesquiterpene, achieved a titer of 34.6 g/L, very close to the reported titer of the similar bicyclic sesquiterpene amorpha-4,11-diene. Benefitting from the high titer in fed-batch fermentation, we easily obtained this compound for deep characterization of its aroma and bioactivity. The unique fragrance of (−)-eremephilene may boost the slow release of the dominant aroma of β-caryophyllene and α-humulene in Holy basil. The mixture of these constituents could naturally form the characteristic fragrance that Holy basil emits. In particular, the significant deterrent efficacy of (−)-eremephilene against the pest, fall leafworm (*Spodoptera frugiperda*), suggests that it could be a promising alternative to synthetic insecticides from plant-derived natural products.

In conclusion, our work presents a promising approach that can be utilized for the bulk mining of sesquiterpene synthases and realizes high-yield production of high-value sesquiterpenes that are difficult to extract or synthesize via regio- and stereoselective chemosynthesis. This study confirms the suitability of expressing terpene synthases using our efficient precursor-producing yeast system. Using this system, we identified six active sesquiterpenes from Holy basil, including the dominant sesquiterpenoid components β-caryophyllene and its close isomer, α-humulene. We also identified the sesquiterpene-synthesizing enzyme, OsaTPS07. The structure of the OsaTPS07 product was identified as (−)-eremophilene for the first time. Then, we evaluated the unique aroma of this compound and determined that (−)-eremophilene has considerable repellant bioactivity against fall leafworms. Our study shows that our heterologous robust precursor supply platform can accelerate the application of diverse plant terpene synthases and their synthesis products. Our (−)-eremophilene biomanufacturing approach promises to provide green and sustainable solutions for stable and scalable requirements through renewable resource consumption and provides a promising alternative to produce plant-derived natural chemicals compared to direct phytoextraction.

4. Materials and methods

4.1. Strains, medium, and chemicals

S. cerevisiae YZL141 and JCR27 reported previously were the background strains for the constructs (Ma et al., 2019; Siemon et al., 2020). Mutant strains were selected on SC medium [0.67% yeast nitrogen base (YNB), proper amino acid drop-out mix and 2% glucose]. YPDG medium (with 1% galactose) was used for yeast cultivation. DNA polymerase was purchased from Takara (Beijing, China). Restriction endonucleases and T4 ligase were respectively purchased from Thermo Fisher Scientific (Waltham, MA) and New England BioLabs (Ipswich, MA). The primers were purchased from GENECREATE (Wuhan, China). The authorized standard α-humulene (J&K Scientific, #562868, CAS: 6753-98-6), *trans*-nerolidol (Sigma-Aldric/Merck, #18143, CAS: 40716-66-3), β-caryophyllene (Macklin, #C832338, CAS: 87-44-5) and valencene (Sigma-Aldric/Merck, #75056, CAS:4630-07-3) were purchased from the commercial chemical companies.

4.2. Bioinformatic analysis of the sesquiterpene synthase from Ocimum sanctum

The amino acids of the fourteen sesquiterpene synthases (OsaTPS01, OsaTPS2, OsaTPS04, OsaTPS05, OsaTPS07, OsaTPS08, OsaTPS09, OsaTPS10, OsaTPS11, OsaTPS12, OsaTPS20, OsaTPS22, OsaTPS23, and OsaTPS44) from *Ocimum sanctum* were aligned by ClustW. A maximum-likelihood phylogenetic tree was generated by using MEGA-X software based on the Jones-Taylor-Thornton matrix-based model. The conserved motifs of the sesquiterpene synthases from Holy basil were aligned by ClustW and subsequently analyzed by ESPript 3 (Robert and Gouet, 2014).

4.3. Evaluation of the Holy basil sesquiterpene synthases in yeasts

The coding regions of *OsaTPS01*, *OsaTPS2*, *OsaTPS04*, *OsaTPS05*, *OsaTPS07*, *OsaTPS08*, *OsaTPS09*, *OsaTPS10*, *OsaTPS11*, *OsaTPS12*, *OsaTPS20*, *OsaTPS22*, *OsaTPS23*, and *OsaTPS44* genes were optimized and introduced into the yeast vector pRS426 under the GAL1 promoter. The recombinant plasmids were transformed into YZL141 to generate yeast mutant strains JVA41, JVA29, and JVA30 and JDX1-11. The culture conditions were according to the methods described previously (Ma

et al., 2019). Briefly, the mutant yeasts were inoculated in 5 mL of SC-URA medium at 30°C overnight. Thereafter, approximately 0.5 ml strains were added into 50 mL of YPDG in a 250 mL shaken-flask for another 3-d cultivation at 30°C. Finally, the strains were harvested and extracted with an equal volume of hexane three times. The organic layer was then applied for GC-MS detection.

4.4. Functional characterization in Escherichia coli

The coding region of the *OsaTPS07* was inserted into the *Nco*I/*Xho*I restriction site of the pET32a (+) vector (Merck Millipore) to generate plasmid pDX012. The plasmid was transformed into BL21 (DE3) and cultivated in LB medium overnight at 37°C. Thereafter, 0.5 mM isopropyl-1-thio-*β*-D-galactopyranoside (IPTG) was used to induce recombinant protein expression when the OD600 reached approximately 0.6 and further cultivation at 16°C overnight. Cells were collected and resuspended in Buffer A, subsequently lysed by ultrasonication and the soluble proteins in the supernatant were purified by Ni-NTA affinity chromatography column and assayed by SDS-PAGE. In vitro enzyme assay was carried out in 200 μL reaction buffer (PBS, 2 mM Mg^{2+}) typically containing 50 μg of purified proteins and 10 μM FPP at 30°C overnight. The reaction products were extracted by hexane for GC-MS analysis, the negative control without the targeted recombinant protein and the positive standard valencene were also performed GC-MS analysis.

4.5. Construction of the plasmids and yeast mutants

The primer sequences used for desired plasmids were listed in Supplementary Table S1. All strains and plasmids are summarized in Supplementary Tables S2 and S3. The fourteen Holy Basil sesquiterpene synthases genes were referred to the previous study (Kumar et al., 2018). The *OsaTPS08* gene was amplified by PCR using high-fidelity DNA Polymerase with gene-specific primers P1/P2, the common expression cassette including *ERG20* gene was amplified using primers P3/P4 from the pZY141 plasmid described before (Ma et al., 2019) and used as the same fragment for subsequent plasmids construction. The *OsaTPS08* gene fragment and the fragment containing *ERG20* gene and the pRS426 backbone fragment were ligated to form the complete vector pKZ745 by the homologous recombination methods. The pKZ746 and pKZ747 were constructed similarly to pKZ745 using the primers P5/P6 and P7/P8, respectively. The plasmids from pDX001 to pDX011 were constructed similarly with different primers pairs (P9/P10, *OsaTPS01*; P11/P12, *OsaTPS02*; P13/P14, *OsaTPS04*; P15/P16, *OsaTPS05*; P17/P18, *OsaTPS10*; P19/P20, *OsaTPS11*; P21/P22, *OsaTPS12*; P23/P24, *OsaTPS20*; P25/P26, *OsaTPS22*; P27/P28, *OsaTPS23*; P29/P30, *OsaTPS44*). For pDX012 vector construction, the *OsaTPS07* gene was obtained by PCR using primers P31/P32 from the pKZ747 plasmid and was assembled into the expression vector pET32a. The *OsaTPS07* gene fragment, the homologous arm of *URA* loci, the expression cassette fragment containing *HMG1* gene and the fragments including the *HIS* selective gene were obtained respectively using distinctive templates pKZ747 plasmid with primer pairs P33/P34, and pZY161 plasmid with primers P35/P36 and P39/P40, and pZY141 plasmid with primers P37/P38. All these fragments were assembled with the pRS426 backbone fragment to generate another complete vector pHM001. Similarly, the *OsaTPS07* gene expression cassette fragment was amplified with specific primers P41/P42, the *hyg* resistant gene fragment was amplified from pTM36 plasmid with primers P43/P44, the homologous arm of *GAL80* were respectively amplified from the CEN.PK2-1D DNA template with the specific primers P45/P46 and P47/P48. Thereafter, these specific fragments were assembled with the pRS426 backbone fragment to form the pHM003 plasmid. The final fragments containing the homologous arm of *YPRCdelta15* loci and the *URA* and *TRP* genes were obtained from the CEN.PK2-1D DNA using P49/P50, P51/P52, P53/P54, and P55/P56 as specific primer pairs, and from pRS426 or pZY141 plasmids, these fragments were used for the subsequent templates for homologous recombination.

For preliminary *OsaTPS07* expression cassette insertion in the platform strain JCR27, the abovementioned pKZ747 plasmid was digested by *Pme*I restriction enzyme, the purified fragment containing the correct *OsaTPS07* gene expression cassette was further transformed into JCR27 strain by PEG/LiCl method and the correct recombinant strains were confirmed by colony-PCR and sequencing, thus generated the first-generation yeast mutant strain JHM1. Another copy of the *OsaTPS07* expression cassette was achieved by digestion of the pHM001 plasmid with *Pme*I, followed by an introduction of the correct new *OsaTPS07* gene expression cassette into the JHM1 strain via homologous recombination. The resultant second-generation strain JHM2 was denoted after colony-PCR and sequencing confirmation. JHM3 was constructed after the excision of the *hyg* resistant gene for its subsequent recycled. The JHM4 strain was obtained by inserted the correct fragment containing an extra copy of *OsaTPS07* gene expression cassette after digestion of the pHM003 by *Pme*I with the same methods mentioned above. Finally, the JHM5 mutant strain was supplemented with the *URA* and *TRP* expressions genes by introducing the fragment that bearing the *YPRCdelta15* homologues arms via PEG/LiCl transformation method.

4.6. Shake-flask fermentation

Recombinant strains were activated on the plate and inoculated into 5 mL of YPD medium for further overnight cultivation at 30°C. Thereafter, approximately 0.5 ml strains were added into 50 mL of YPDG in 250 mL shaken-flask for another 3-d cultivation at 30°C. The estergel was used as an organic extractant. Cell growth was measured at the fermentation end-point.

4.7. Fed-batch fermentation

4.7.1. Fermentation in 1-L bioreactor for strain characterization

For strain characterization, a 1-L parallel bioreactor (T&J-Mini Box 1L*8, Shanghai T&J Bio-engineering Co., LTD) containing a 300 mL batch medium was adopted. The media used for this work were derived from the process described previously (Shi et al., 2019). The complete synthetic medium (CSM) contained per liter: glucose 40 g, $(NH_4)_2SO_4$ 15 g, KH_2PO_4 8 g, $MgSO_4•7H_2O$ 6.15 g, vitamin solution 12 mL, trace metals solution 10 mL, $NH_3•H_2O$ was used to adjust pH to 5.0. Vitamin solution contained per liter: biotin 0.05 g, calcium pantothenate 1 g, nicotinic acid 1 g, myo-inositol 25 g, thiamine •HCl 1g, pyridoxal •HCl 1 g, and *p*-aminobenzoic acid 0.2 g. Trace metals solution contained per liter: EDTA 15 g, $ZnSO_4•7H_2O$ 5.75 g, $MnCl_2•4H_2O$ 0.32 g, anhydrous $CuSO_4$ 0.5 g, $CoCl_2•6H_2O$ 0.47 g, $Na_2MoO_4•2H_2O$ 0.48 g, $CaCl_2•2H_2O$ 2.9 g, $FeSO_4•7H_2O$ 2.8 g.

The engineered yeast strain precultured in the CSM medium with 50 mM succinate (pH 5.0) was used as the seed culture. To obtain the seed culture, single colonies were grown in 5 mL CSM medium overnight at 30°C, 220 rpm, after which 1% of the seed culture was transferred to a 500-mL flask containing 200 mL CSM medium and cultured at 30°C with shaking at 220 rpm for 16 h–18 h. 10% of the seed culture was then inoculated into 300 mL CSM medium in the fermentor for fed-batch fermentation at 30°C. The dissolved oxygen was kept at about 20% by adjusting the agitation speed from 200 to 700 rpm and the airflow rate from 1 vvm-2vvm. The pH was controlled at 5.0 by the automatic addition of $NH_3•H_2O$.

A two-stage fed-batch strategy was employed according to the GAL-regulation system for (−)-eremophilene bioproduction. When the residual glucose was below 1 g/L, the feeding solution I consisting of 500 g/L glucose, 9 g/L KH_2PO_4, 5.12 g/L $MgSO_4$, 3.5 g/L K_2SO_4, 0.28 g/L Na_2SO_4 was used to ensure rapid cell growth. The feeding rate was adjusted to control the glucose concentration by about 1 g/L. When OD reached 150, the solution I feeding was stopped, and the culture was overlaid with estergel (20% volume) to facilitate (−)-eremophilene

accumulation. During the second feeding stage, feeding solution II ethanol was used as the carbon source to stimulate the (−)-eremophilene accumulation. Ethanol residual concentration was controlled by about 5 g/L by adjusting the solution II feeding rate. The fermentation stopped when the (−)-eremophilene titer was not increasing.

4.7.2. Fermentation in 15-L fermentor for (−)-eremophilene overproduction

After strain evaluation in a 1-L bioreactor, the fermentation scale was enlarged to a 15-L stainless steel fermentor. Fermentation medium and process control are essentially the same as in the 1-L bioreactor. The difference is that there is a pressure in the steel fermentor, which is maintained at 0.03–0.04 MPa during fermentation.

4.8. Metabolite extraction and analysis

Glucose and ethanol concentrations were determined by a Bio-analyzer (SBA-40C, Shandong Academy of Sciences, China) according to the standard instructions. The yield of the targeted sesquiterpene was quantified using the valencene and (−)-eremophilene as the quantitation standard.

To determine the fine chemical structure of the product of OsaTPS07, the crude extracts were initially purified by silica gel column chromatography using petroleum ether/ethyl acetate. The refined compound was obtained using an Ultimate 3000 HPLC equipment with RP C18 column. The distinct peaks were confirmed by GC-MS. The refined compound was finally analyzed by NMR. The optical activity and optical rotation were analyzed by Rudolph Research Analytical Autopol IV Automatic Polarimeter in $CDCl_3$ solution.

The GC-MS assessment was performed on Thermo TRACE GC Ultra combined with a TSQ Quantum XLS MS. The oven temperature was initially set at 50°C for 1 min, increased to 280°C at 15°C/min, held for 1 min, then subsequently increased to 300°C at 20°C/min, and held for 2 min. The injector and transfer lines were maintained at 240°C and 270°C, respectively. Compounds were identified by comparison with the NIST database (National Institute of Standards and Technology) library and the retention indices (Fang et al., 2017).

1D and 2D NMR data were recorded using an Agilent (Santa Clara, CA, USA) DD2NMR spectrometer (400 MHz or 600 MHz). $CDCl_3$ was used for NMR measurements. Chemical shifts were recorded in ppm downfield from tetramethylsilane. The shifts for ^{1}H-NMR were reported relative to the proton resonance of $CHCl_3$. The shifts for ^{13}C-NMR were reported relative to the carbon resonance of $CDCl_3$. The chemical shift, multiplicity (s = singlet, d = doublet, t = triplet, q = quartet, m = multiplet, br = broad), coupling constant (Hz), and integration were recorded as well.

4.9. Bioactivity assay

The antifeedant activity of (−)-eremophilene to the injurious insect was conducted according to the methods (Chen et al., 2002; Luo et al., 2020). The leaf disc dipping method was carried out to evaluate the antifeedant activity of the (−)-eremophilene. The insect corn leafworm (*Spodoptera frugiperda*) was bred and used for the bioactivity assay in Plant Protection Research Institute, Guangdong Academy of Agricultural Sciences. The compound (−)-eremophilene was dissolved in acetone and five concentration gradients 50, 100, 200, 500, and 800 μg/mL were tested. The tested fresh peanut (*Arachis hypogaea*) leaf discs were cut by a borer (15 mm in diameter) and painted in the above five acetone solutions respectively for 5 s, the control leaf discs were treated with acetone alone as well. Then, two control leaf discs and two tested ones were placed together in alternating permutation in the Petri dish (150 mm in diameter). Thereafter, 3rd instar larvae that were starved for 6 h were put at the center of the above Petri dish. Each treatment was tested with five replicates. The feeding areas of the leaf discs were measured when feeding for 24 h. The selective antifeedant rate (%) is calculated as (C−T)/(C + T) × 100, where C refers to the average feeding area of the control group and T refers to the average feeding area of the treated group. The statistical analysis was performed by using SPSS19.0 and Duncan's new multiple range test.

CRediT authorship contribution statement

Xiaomin Deng: Conceptualization, Methodology, Validation, Investigation, Resources, Funding acquisition, Formal analysis, Writing – original draft, Visualization. **Bin Shi:** Methodology, Formal analysis, Writing – original draft, Visualization. **Ziling Ye:** Methodology, Resources. **Man Huang:** Methodology, Validation. **Rong Chen:** Methodology, Formal analysis. **Yousheng Cai:** Formal analysis. **Zhaolin Kuang:** Validation, Investigation. **Xiang Sun:** Methodology. **Guangkai Bian:** Methodology, Resources. **Zixin Deng:** Resources, Supervision. **Tiangang Liu:** Conceptualization, Resources, Funding acquisition, Supervision, Writing – review & editing.

Declaration of competing interest

The authors are applying of a series patents base on this work.

Acknowledgments

We would like to thank Yanxia Zuo (The Analysis and Testing Center of the Institute of Hydrobiology, Chinese Academy of Sciences) for technical assistance in detecting the (−)-eremophilene. We also thank Chuanying Li and Pingyu Zhang (Plant Protection Research Institute, Guangdong Academy of Agricultural Sciences/Guangdong Provincial Key Laboratory of High Technology for Plant Protection, China) for assistance in antifeeding activity analysis. We also thank the Analytical & Measuring Center, School of Pharmaceutical Sciences, South-Central University for Nationalities for spectra measurements of the (−)-eremophilene.

Appendix A. Supplementary data

Supplementary data to this article can be found online at https://doi.org/10.1016/j.ymben.2021.11.005.

Funding

This work is financially supported by grants from J1 Biotech Co.Ltd. (J1-030), and the National Key Research and Development Program of China (2018YFA0900400), and Hainan Provincial Natural Science Foundation of China (320RC734), and Hubei Province Postdoctoral Innovation Practice Post Project ([2019] No.2).

References

Ahmed, M., Peiwen, Q., Gu, Z., Liu, Y., Sikandar, A., Hussain, D., Javeed, A., Shafi, J., Iqbal, M.F., An, R., Guo, H., Du, Y., Wang, W., Zhang, Y., Ji, M., 2020. Insecticidal activity and biochemical composition of *Citrullus colocynthis, Cannabis indica* and *Artemisia argyi* extracts against cabbage aphid (*Brevicoryne brassicae* L.). Sci. Rep. 10, 522. https://doi.org/10.1038/s41598-019-57092-5.

Alquézar, B., Volpe, H.X.L., Magnani, R.F., de Miranda, M.P., Santos, M.A., Marques, V. V., de Almeida, M.R., Wulff, N.A., Ting, H.M., de Vries, M., Schuurink, R., Bouwmeester, H., Peña, L., 2021. Engineered orange ectopically expressing the Arabidopsis β-caryophyllene synthase is not attractive to *Diaphorina citri*, the vector of the bacterial pathogen associated to huanglongbing. Front. Plant Sci. 12, 641457. https://doi.org/10.3389/fpls.2021.641457.

Belcher, M.S., Mahinthakumar, J., Keasling, J.D., 2020. New frontiers: harnessing pivotal advances in microbial engineering for the biosynthesis of plant-derived terpenoids. Curr. Opin. Biotechnol. 65, 88–93. https://doi.org/10.1016/j.copbio.2020.02.001.

Beekwilder, J., van Houwelingen, A., Cankar, K., van Dijk, A.D., de Jong, R.M., Stoopen, G., Bouwmeester, H., Achkar, J., Sonke, T., Bosch, D., 2014. Valencene synthase from the heartwood of Nootka cypress (*Callitropsis nootkatensis*) for biotechnological production of valencene. Plant Biotechnol. J. 12, 174–182. https://doi.org/10.1111/pbi.12124.

Bian, G.K., Han, Y.C., Hou, A.W., Yuan, Y.J., Liu, X.H., Deng, Z.X., Liu, T.G., 2017. Releasing the potential power of terpene synthases by a robust precursor supply platform. Metab. Eng. 42, 1–8. https://doi.org/10.1016/j.ymben.2017.04.006.

Bleeker, P.M., Spyropoulou, E.A., Diergaarde, P.J., Volpin, H., De Both, M.T., Zerbe, P., Bohlmann, J., Falara, V., Matsuba, Y., Pichersky, E., Haring, M.A., Schuurink, R.C., 2011. RNA-seq discovery, functional characterization, and comparison of sesquiterpene syn thases from *Solanum lycopersicum* and *Solanum habrochaites* trichomes. Plant Mol. Biol. 77, 323–336. https://doi.org/10.1007/s11103-011-9813-x.

Burkhardt, I., Siemon, T., Henrot, M., Studt, L., Rösler, S., Tudzynski, B., Christmann, M., Dickschat, J.S., 2016. Mechanistic characterisation of two sesquiterpene cyclases from the plant pathogenic fungus *Fusarium fujikuroi*. Angew Chem. Int. Ed. Engl. 55, 8748–8751. https://doi.org/10.1186/s12934-019-1246-2.

Chen, D.M., Zhang, Z.X., Xu, H.H., Wu, Y.L., Fan, J.F., 2002. Antifeedant activity of spiro enol ether analogues against vegetable insects. J. Huazhong Archit. Univ. 21, 343–346.

Chen, R., Jia, Q., Mu, X., Hu, B., Sun, X., Deng, Z., Chen, F., Bian, G., Liu, T., 2021. Systematic mining of fungal chimeric terpene synthases using an efficient precursor-providing yeast chassis. Proc. Natl. Acad. Sci. U.S.A. 118, e2023247118 https://doi.org/10.1073/pnas.2023247118.

Coates, R.M., Shaw, J.E., 1970. Stereoselective total synthesis of (+-)-eremoligenol, (+-)-eremophilene, (+-)-valerianol, and (+-)-valencene. J. Org. Chem. 35, 2597–2601.

da Silva, R.C., Milet-Pinheiro, P., Bezerra da Silva, P.C., da Silva, A.G., da Silva, M.V., Navarro, D.M., da Silva, N.H., 2015. (*E*)-Caryophyllene and α-humulene: *Aedes aegypti* oviposition deterrents elucidated by gas chromatography-electrophysiological assay of *Commiphora leptophloeos* leaf oil. PLoS One 10, e0144586. https://doi.org/10.1371/journal.pone.0144586.

Falara, V., Akhtar, T.A., Nguyen, T.T., Spyropoulou, E.A., Bleeker, P.M., Schauvinhold, I., Matsuba, Y., Bonini, M.E., Schilmiller, A.L., Last, R.L., Schuurink, R.C., Pichersky, E., 2011. The tomato terpene synthase gene family. Plant Physiol. 157, 770–789. https://doi.org/10.1104/pp.111.179648.

Fang, X., Li, C.Y., Yang, Y., Cui, M.Y., Chen, X.Y., Yang, L., 2017. Identification of a novel (-)-5-Epieremophilene synthase from *Salvia miltiorrhiza* via transcriptome mining. Front. Plant Sci. 8, 627. https://doi.org/10.3389/fpls.2017.00627.

Greenhagen, B.T., O'Maille, P.E., Noel, J.P., Chappell, J., 2006. Identifying and manipulating structural determinates linking catalytic specificities in terpene synthases. Proc. Natl. Acad. Sci. U.S.A. 103, 9826–9831. https://doi.org/10.1073/pnas.0601605103.

Gupta, S.K., Prakash, J., Srivastava, S., 2002. Validation of traditional claim of Tulsi. *Ocimum sanctum* Linn. as a medicinal plant. Indian J. Exp. Biol. 40, 765–773.

Jamshidi, N., Cohen, M.M., 2017. The clinical efficacy and safety of tulsi in humans: a systematic review of the literature. Evid. Based Complement Alternat. Med. 2017, 9217567. https://doi.org/10.1155/2017/9217567.

Ko, Y.S., Kim, J.W., Lee, J.A., Han, T., Kim, G.B., Park, J.E., Lee, S.Y., 2020. Tools and strategies of systems metabolic engineering for the development of microbial cell factories for chemical production. Chem. Soc. Rev. 49, 4615–4636. https://doi.org/10.1039/d0cs00155d.

Krepinsky, J., Motl, O., Dolejs, L., Novotny, L., Herout, V., Bates, R.B., 1968. The structure of eremophilene, the sesquiterpenic hydrocarbon from *Petasites genus*. Tetrahedron Lett. 29, 3315–3318.

Kumar, Y., Khan, F., Rastogi, S., Shasany, A.K., 2018. Genome-wide detection of terpene synthase genes in holy basil (*Ocimum sanctum* L.). PLoS One 13, e0207097. https://doi.org/10.1371/journal.pone.0207097.

Li, W., Yan, X., Zhang, Y., Liang, D., Caiyin, Q., Qiao, J., 2021. Characterization of *trans*-nerolidol synthase from *Celastrus angulatus* maxim and production of *trans*-nerolidol in engineered *Saccharomyces cerevisiae*. J. Agric. Food Chem. 69, 2236–2244. https://doi.org/10.1021/acs.jafc.0c06084.

Liu, M., Lin, Y.C., Guo, J.J., Du, M.M., Tao, X., Gao, B., Zhao, M., Ma, Y., Wang, F.Q., Wei, D.Z., 2021. High-level production of sesquiterpene patchoulol in *Saccharomyces cerevisiae*. ACS Synth. Biol. 10, 158–172. https://doi.org/10.1021/acssynbio.0c00521.

Lücker, J., Bowen, P., Bohlmann, J., 2004. *Vitis vinifera* terpenoid cyclases: functional identification of two sesquiterpene synthase cDNAs encoding (+)-valencene synthase and (-)-germacrene D synthase and expression of mono- and sesquiterpene synthases in grapevine flowers and berries. Phytochemistry 65, 2649–2659. https://doi.org/10.1016/j.phytochem.2004.08.017.

Luo, L.Q., Chen, Y.G., Li, D.S., Liu, Y., Li, S.H., 2020. Production of the inaccessible sesquiterpene (-)-5-Epieremophilene by metabolically engineered *Escherichia coli*. Chem. Biodivers. 17, e2000219 https://doi.org/10.1002/cbdv.202000219.

Ma, T., Shi, B., Ye, Z., Li, X., Liu, M., Chen, Y., Xia, J., Nielsen, J., Deng, Z., Liu, T., 2019. Lipid engineering combined with systematic metabolic engineering of *Saccharomyces cerevisiae* for high-yield production of lycopene. Metab. Eng. 52, 134–142. https://doi.org/10.1016/j.ymben.2018.11.009.

Mateos Fernández, R., Petek, M., Gerasymenko, I., Juteršek, M., Baebler, Š., Kallam, K., Moreno Giménez, E., Gondolf, J., Nordmann, A., Gruden, K., Orzaez, D., Patron, N.J., 2021. Insect pest management in the age of synthetic biology. Plant Biotechnol. J. https://doi.org/10.1111/pbi.13685.

Meadows, A.L., Hawkins, K.M., Tsegaye, Y., Antipov, E., Kim, Y., Raetz, L., Dahl, R.H., Tai, A., Mahatdejkul-Meadows, T., Xu, L., Zhao, L., Dasika, M.S., Murarka, A., Lenihan, J., Eng, D., Leng, J.S., Liu, C.L., Wenger, J.W., Jiang, H., Chao, L., Westfall, P., Lai, J., Ganesan, S., Jackson, P., Mans, R., Platt, D., Reeves, C.D., Saija, P.R., Wichmann, G., Holmes, V.F., Benjamin, K., Hill, P.W., Gardner, T.S., Tsong, A.E., 2016. Rewriting yeast central carbon metabolism for industrial isoprenoid production. Nature 537, 694–697. https://doi.org/10.1038/nature19769.

Padalia, R.C., Verma, R.S., 2011. Comparative volatile oil composition of four Ocimum species from northern India. Nat. Prod. Res. 25, 569–575. https://doi.org/10.1080/14786419.2010.482936.

Paddon, C.J., Westfall, P.J., Pitera, D.J., Benjamin, K., Fisher, K., McPhee, D., Leavell, M. D., Tai, A., Main, A., Eng, D., Polichuk, D.R., Teoh, K.H., Reed, D.W., Treynor, T., Lenihan, J., Fleck, M., Bajad, S., Dang, G., Dengrove, D., Diola, D., Dorin, G., Ellens, K.W., Fickes, S., Galazzo, J., Gaucher, S.P., Geistlinger, T., Henry, R., Hepp, M., Horning, T., Iqbal, T., Jiang, H., Kizer, L., Lieu, B., Melis, D., Moss, N., Regentin, R., Secrest, S., Tsuruta, H., Vazquez, R., Westblade, L.F., Xu, L., Yu, M., Zhang, Y., Zhao, L., Lievense, J., Covello, P.S., Keasling, J.D., Reiling, K.K., Renninger, N.S., Newman, J.D., 2013. High-level semi-synthetic production of the potent antimalarial artemisinin. Nature 496, 528–532. https://doi.org/10.1038/nature12051.

Rastogi, S., Kalra, A., Gupta, V., Khan, F., Lal, R.K., Tripathi, A.K., Parameswaran, S., Gopalakrishnan, C., Ramaswamy, G., Shasany, A.K., 2015. Unravelling the genome of Holy basil: an "incomparable" "elixir of life" of traditional Indian medicine. BMC Genom. 16, 413. https://doi.org/10.1186/s12864-015-1640-z.

Robert, X., Gouet, P., 2014. Deciphering key features in protein structures with the new ENDscript server. Nucleic Acids Res. 42, W320–324. https://doi.org/10.1093/nar/gku316.

Schifrin, A., Ly, T.T., Günnewich, N., Zapp, J., Thiel, V., Schulz, S., Hannemann, F., Khatri, Y., Bernhardt, R., 2015. Characterization of the gene cluster CYP264B1-geoA from *Sorangium cellulosum* So ce56: biosynthesis of (+)-eremophilene and its hydroxylation. Chembiochem 16, 337–344. https://doi.org/10.1002/cbic.201402443.

Sharon-Asa, L., Shalit, M., Frydman, A., Bar, E., Holland, D., Or, E., Lavi, U., Lewinsohn, E., Eyal, Y., 2003. Citrus fruit flavor and aroma biosynthesis: isolation, functional characterization, and developmental regulation of *Cstps1*, a key gene in the production of the sesquiterpene aroma compound valencene. Plant J. 36, 664–674. https://doi.org/10.1046/j.1365-313x.2003.01910.x.

Shi, B., Ma, T., Ye, Z., Li, X., Huang, Y., Zhou, Z., Ding, Y., Deng, Z., Liu, T., 2019. Systematic metabolic engineering of *Saccharomyces cerevisiae* for lycopene overproduction. J. Agric. Food Chem. 67, 11148–11157. https://doi.org/10.1021/acs.jafc.9b04519.

Siemon, T., Wang, Z., Bian, G., Seitz, T., Ye, Z., Lu, Y., Cheng, S., Ding, Y., Huang, Y., Deng, Z., Liu, T., Christmann, M., 2020. Semisynthesis of plant-derived Englerin A enabled by microbe engineering of guaia-6,10(14)-diene as building block. J. Am. Chem. Soc. 142, 2760–2765. https://doi.org/10.1021/jacs.9b12940.

Tangpao, T., Chung, H.H., Sommano, S.R., 2018. Aromatic profiles of essential oils from five commonly used Thai basils. Foods 7, 175. https://doi.org/10.3390/foods7110175.

Wang, J., Jiang, W., Liang, C., Zhu, L., Li, Y., Mo, Q., Xu, S., Chu, A., Zhang, L., Ding, Z., Shi, G., 2021. Overproduction of α-farnesene in *Saccharomyces cerevisiae* by farnesene synthase screening and metabolic engineering. J. Agric. Food Chem. 69, 3103–3113. https://doi.org/10.1021/acs.jafc.1c00008.

Westfall, P.J., Pitera, D.J., Lenihan, J.R., Eng, D., Woolard, F.X., Regentin, R., Horning, T., Tsuruta, H., Melis, D.J., Owens, A., Fickes, S., Diola, D., Benjamin, K.R., Keasling, J.D., Leavell, M.D., McPhee, D.J., Renninger, N.S., Newman, J.D., Paddon, C.J., 2012. Production of amorphadiene in yeast, and its conversion to dihydroartemisinic acid, precursor to the antimalarial agent artemisinin. Proc. Natl. Acad. Sci. U.S.A. 109, E111–E118. https://doi.org/10.1073/pnas.1110740109.

Xie, W., Lv, X., Ye, L., Zhou, P., Yu, H., 2015. Construction of lycopene-overproducing *Saccharomyces cerevisiae* by combining directed evolution and metabolic engineering. Metab. Eng. 30, 69–78. https://doi.org/10.1016/j.ymben.2015.04.009.

Xu, H., Dickschat, J.S., 2020. GermacreneA-ACentral intermediate in sesquiterpene biosynthesis. Chemistry 26, 17318–17341. https://doi.org/10.1002/chem.202002163.

Zhang, Y., Zhou, L., Tang, K., Xu, M., Miao, Z., 2020. Matching is the key factor to improve the production of patchoulol in the plant chassis of *Marchantia paleacea*. ACS Omega 5, 33028–33038. https://doi.org/10.1021/acsomega.0c04391.

Zhao, H., Jiang, F.T., Yang, Y.X., Zhang, W., Liu, X.H., 2004a. Analysis of the essential oil from *Aristolochia mollissima* Hance by GC/MS. Henan Daxue Xuebao, Ziran Kexueban. 34, 44–46.

Zhao, Y., Schenk, D.J., Takahashi, S., Chappell, J., Coates, R.M., 2004b. Eremophilane sesquiterpenes from capsidiol. J. Org. Chem. 69, 7428–7435. https://doi.org/10.1021/jo049058c.

Zheljazkov, V.D., Cantrell, C.L., Tekwani, B., Khan, S.I., 2008. Content, composition, and bioactivity of the essential oils of three basil genotypes as a function of harvesting. J. Agric. Food Chem. 56, 380–385. https://doi.org/10.1021/jf0725629.

Zhou, F., Pichersky, E., 2020. The complete functional characterisation of the terpene synthase family in tomato. New Phytol. 226, 1341–1360. https://doi.org/10.1111/nph.16431.